pnCCDs for Ultra-Fast and Ultra-Sensitive Optical and NIR Imaging

Peter Holl[*,†], Robert Hartmann[*,†], Sebastian Ihle[*,†], Gottfried Kanbach[**], Gerhard Lutz[*,†], Ivan Ordavo[*,†], Heike Soltau[*], Alexander Stefanescu[**] and Lothar Strüder[**,†]

[*] *PNSensor GmbH, Römerstraße 28, 80803 München, Germany*
[†] *MPI Halbleiterlabor, Otto-Hahn-Ring 6, 81739 München, Germany*
[**] *Max-Planck-Institut für extraterrestrische Physik, Giessenbachstraße, 85748 Garching, Germany*

Abstract. We present the design, status of fabrication and testing, and expected performance characteristics of new CCDs for highest frame rates and excellent sensitivity over a wide wavelength range, from the near UV to the to near IR. To achieve frame rates in the kHz regime, the devices are based on proven technology with column parallel readout. The CCDs are back illuminated, sensitive over their full thickness of 450 µm, allowing a peak quantum efficiency near 100 % at any chosen wavelength between 400 nm and 1,000 nm.

Test results, including astronomical trials at Skinakas observatory, using available devices with an on-chip JFET amplifier are presented. Based on the above CCD design we are currently producing two novel variants with single photon counting capabilities: They either use integrated avalanche diodes in the readout chain or a repetitive non-destructive readout. Both readout schemes have already successfully proven their single-photon sensitivity and we present the related results.

Keywords: Silicon Detector, CCD, Single Photon Counting, High Frame Rate Imaging, Near Infrared Sensitivity
PACS: 85.60.Gz

1. INTRODUCTION

We are developing new optical CCD detectors which shall allow single photon imaging at highest frame rates (in the kilohertz regime) and with quantum efficiency near 100 % in selected wavelength ranges from the near UV to the near infrared. Apart from any other low light level application, this device is particularly useful as a focal plane instrument in High Time Resolution Astronomy (HTRA) and as a wavefront sensor for Adaptive Optics.

The Max-Planck-Institut Halbleiterlabor (semiconductor laboratory) pursues two different strategies to realize detection of single optical photons. One is to lower the detector noise to the sub-electron level. This is achieved by repetitive non-destructive read-out (RNDR, [2]). While this method is very promising and delivers high dynamics and linearity, it is not yet suitable for fast imaging. The second strategy, which is described in this article, uses avalanche multiplication to increase the signals from single photons (usually one or two electrons) above the noise level.

In Section 2 we describe the general concept of avalanche CCDs. It is followed by test results from various components which define the performance of the device: Section 3 is dedicated to CCD performance and applications in optical astronomy, Section 4 to the

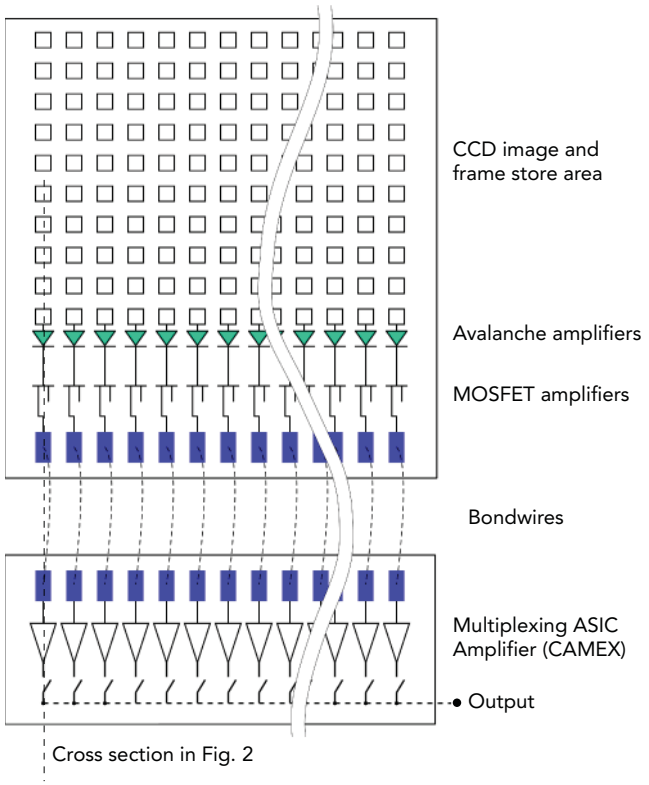

FIGURE 1. Schematic view (not to scale) of a pnCCD with avalanche readout

optical properties of the entrance window and Section 5 to the avalanche readout. The status of the project and its future are summarized in the conclusions.

2. AVALANCHE CCD CONCEPT

Figure 1 shows the building blocks of a single photon sensitive CCD. An image store area represents the sensitive area and consists typically of 256 × 256 pixels. It is coupled to a frame store area with equal number of pixels. The columns are read out in parallel through multiplexing ASIC amplifiers which makes the device very fast. Using 4 output nodes the CCD can be read at rates exceeding 1000 full frames/s. Figure 2 shows a cross section of the last registers and the readout region. The charge is transferred from left to right at a depth of about 3 µm by a three phase register structure. The last transfer occurs from the CCD area to the avalanche cell, where the electron is accelerated by the electric field, which has to be high enough to sustain avalanche multiplication. The fast signal is then coupled to the gate of an on-chip n-channel MOSFET transistor in source follower configuration. Self-quenching of the current is achieved through a high value resistor (R_Q>1 MΩ), realized on-chip by a resistive layer.

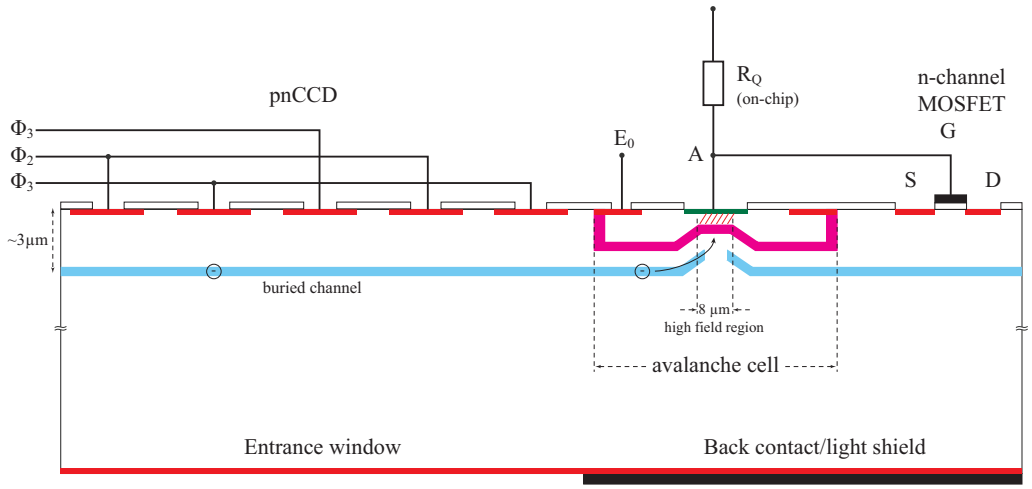

FIGURE 2. Cross section (not to scale) of a pnCCD with avalanche readout

3. PNCCD PERFORMANCE

3.1. CCD Leakage Current Optimization

In general, the major contribution to dark signals in a fully depleted pnCCD is given by conduction electrons thermally generated in the silicon bulk. Such spurious charge is collected during exposure in the potential wells, along with signal electrons and eventually amplified at the readout node. This noise source is intrinsic to all semiconductor devices. Often it is reduced by cooling to a 'negligible' level, where negligible does not mean that it is even close to zero, but that other noise contributions dominate. However, with an electron multiplication mechanism and single electron sensitivity in the readout chain every electron generates an output signal and current leakage has to be suppressed as much as possible.

Since the level of bulk dark current is directly related to defects in the silicon, dark rates may vary substantially depending upon the quality of the substrate material, prefabrication processing and device fabrication itself. Hence, considerable effort has been made in order to achieve rates as low as possible.

Figure 3 shows the temperature dependance of dark current from three different pnCCDs. The squares are from a "conventional" (in the sense of device fabrication process) 75 µm $\times$ 75 µm pixel size CCD. A significant improvement of more than one order of magnitude was achieved with a 36 µm $\times$ 51 µm pixel geometry (triangles), in which a new optimized process sequence has been applied. The same procedure was also used in the fabrication of a third CCD of the same pixel size (fitted diamonds). The only difference resides in the company which produced the bulk material. A further lowering in the dark rate of at least a factor of two is clearly seen. This is most probably due to the different substrate treatment done by the manufacturer during wafer fabrication.

Data points are obtained first by taking a dark image, then reversing the clock sequence to isolate the readout noise, and finally calibrating the obtained values by means of a ^{55}Fe X-ray source (for further details refer to [1]).

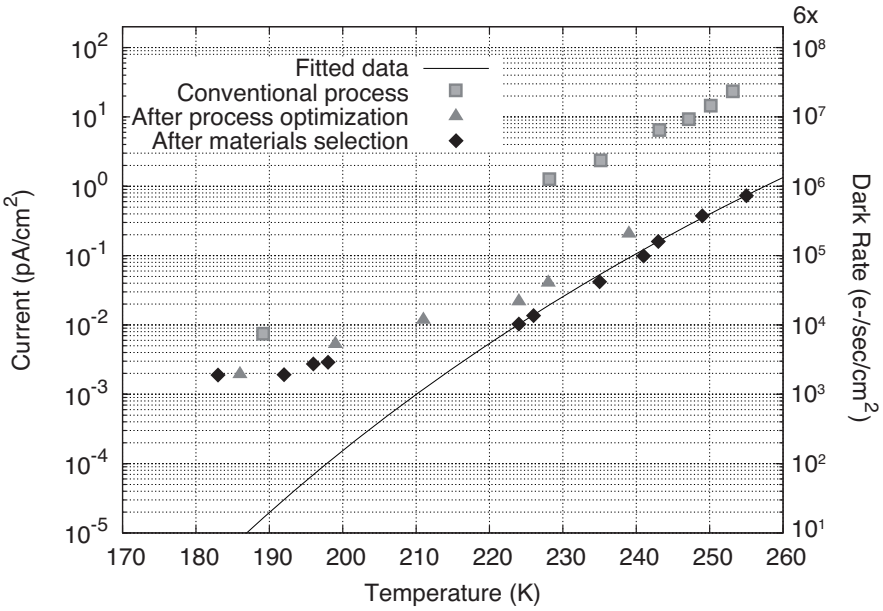

FIGURE 3. Dark current rates for three different devices. Major changes in the device fabrication process led to an overall improvement (upper w.r.t. lower curve) of at least a factor 25. Note how at low temperatures, noise does not further decreases: This is an experimental artefact; dark rate is so low that is not distinguishable any more from other noise sources, primarily readout noise, which become dominant. The solid line indicates the ideal behavior and can be used to extrapolate values even at lower temperatures. All devices have 128 columns and 256 rows of pixels and use column parallel readout.

An interesting specification which can be calculated using the solid line is the doubling temperature, i.e. how many degrees we have to cool the sensor to reduce the dark rate by one-half. Since the theoretical curve is not a straight line, the doubling temperature itself will vary, with the cooling effect becoming more efficient at lower operating temperature. In other words, the effect of a temperature decrease at lower temperatures will result in even larger reduction in dark counts than the same variation applied at higher temperatures. A theoretical value for the doubling temperature at 250 K was found to be 5.76 K, which is in good agreement with the measured one of 6 K $\pm$0.3 K.

Also note from the plot that at low temperatures all curves significantly deviate from the ideal. This is due to the fact that discerning between the very low dark current and readout noise becomes experimentally challenging; basically, the readout noise dominates without decreasing further with temperature. However, the fitted curve gives a clue to which extent dark rate can be lowered. From it, we can extrapolate values as low as 1.5×10^{-4} pA/cm^2 at a temperature of 200 K (-73°C), which translates into 2.4×10^{-2} e$^-$/s/pixel assuming a pixel size of 51 µm $\times$ 51 µm (as actually in production).

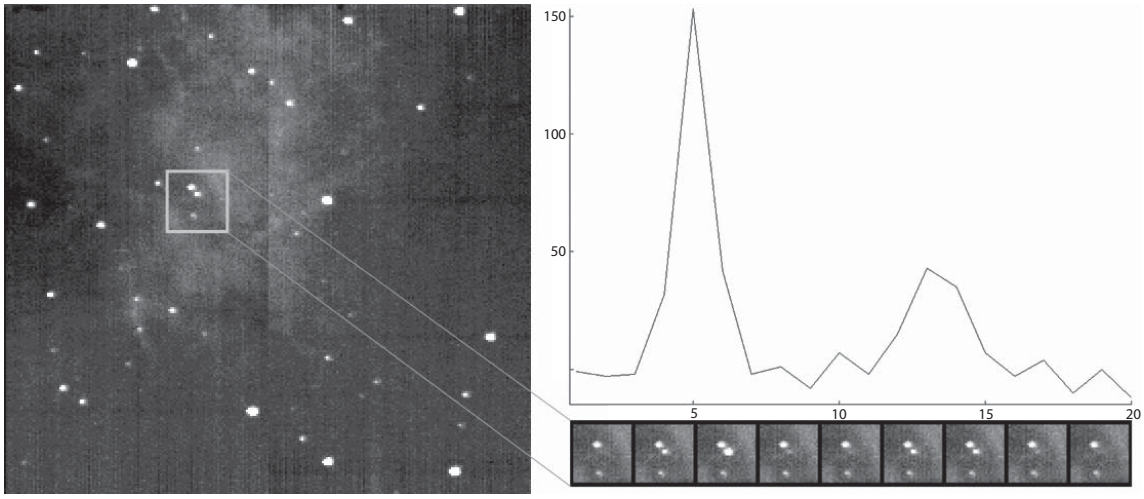

FIGURE 4. Image of the crab nebula (left image) with the pulsar. On the right side, the light curve of the pulsar (approx. 33 ms periode) is resolved with a timing resolution of 1.6 ms. The image sequence underneath the light-curve shows the flickering pulsar and two constant neighboring objects.

3.2. pnCCDs in high-speed astronomical observations

The capabilities of a pnCCD for high-speed optical imaging were tested at the 1.3 m SKINAKAS telescope on the Greek island of Crete. Inaugurated in 1995, the telescope is located 25 km west of Heraklion at an altitude of 1750 m on the Skinakas summit. Its optical system is optimized for high quality wide field imaging to allow the study of extended sky objects like galaxies, star clusters and gaseous nebulas. For a detector a 51 µm pixel-size back illuminated pnCCD detector with a sensitive area of $13 \times 13\,\mathrm{mm}^2$ was used. To allow high speed operations while maintaining the 2-dimensional imaging capabilities, the detector is designed to operate in a split-frame-transfer mode. The imaging area, comprising 264×264 pixels, is split into two halfes to be readout. Each half-image is transferred to its storage region for readout on opposite sides of the detector within 50 µs. During simultaneous readout of the two storage areas, the imaging area is sensitive for incident photons again. That way, the timing resolution of the CCD is given by the time needed to readout and amplify the storage areas. For a readout time of 7 µs per line, a frame repetition rate of nearly 1100 Hz was achieved with an electronic noise floor of less than three electrons ENC at an operating temperature of -55°C. To ensure a high quantum efficiency in the optical and near-infrared region, the radiation entrance window of the detector was equipped with an anti-reflective coating (ARC). With the applied type of ARC, the CCD exhibits a quantum efficiency higher than 80 % between 500 nm and 1000 nm.

As a well studied object for high-speed astronomical photometry the crab nebula with the crab pulsar as central object was observed. Combining the fast variability of the millisecond pulsar (period approx. 33 msec.) with several stars of similar optical magnitudes and the high surface brightness of the nebula in one image, it is excellently suited to demonstrate the ability of a pnCCD to perform high-speed optical, differential photometry over a very large field of view. Shown in Fig. 4 are an image of the nebula as well as a light curve and a time sequence of the pulsar. Both have been obtained after a preliminary analysis of the same data set with a total exposure time of about 30 seconds only. For this observation the pnCCD was operated with a speed of 600 frames per second.

3.3. Effects on Astronomy: Simulations of sources with interstellar reddening

An important figure of merit for a high-time resolution detector is its efficiency, which translates directly into the count rate available from a source. The convolution of an incoming spectrum $F(\nu)$ with the quantum efficiency of the detector $\eta(\nu)$ determines the measured rate of events over a bandwidth (ν_1, ν_2):

$$C = \int_{\nu_1}^{\nu_2} F(\nu) \cdot \eta(\nu)\, d\nu$$

In order to visualize the increase in astronomical 'grasp' that the extended red efficiency of a pnCCD affords we calculate the count rates for unfiltered spectra of typical sources and compare them to the rates in current commercial blue sensitive back-illuminated CCDs with electron multiplication readout (a.k.a. L3 CCDs and EM-CCDs).

Figure 5 shows the generic response curves used in the convolution. For the source spectra we assume non-thermal power-law, as well as thermal black-body spectra. The former because many high-energy sources emit continua of synchrotron radiation (e.g. the Crab pulsar) and the latter because in some applications (e.g. planetary transits or for adaptive optics) normal stellar spectra are observed. The non-thermal spectra are modeled as power laws and the thermal spectra are characterized by their black-body temperature. In addition we consider that an astronomical source is viewed through the interstellar medium, which tends to redden the spectrum. Reddening is described by the color excess E(B-V), i.e. the difference between the blue and visual magnitude which is related to the column depth of the interstellar medium towards the source. Figure 6 displays the gain that can be achieved with a pnCCD detector for a range of power-law and black-body source spectra viewed through different depths of the interstellar medium.

It is quite evident that a gain in count rates up to factors of 5 can be achieved. The higher rates allow division of the observations into shorter temporal bins and still maintain a statistically meaningful analysis.

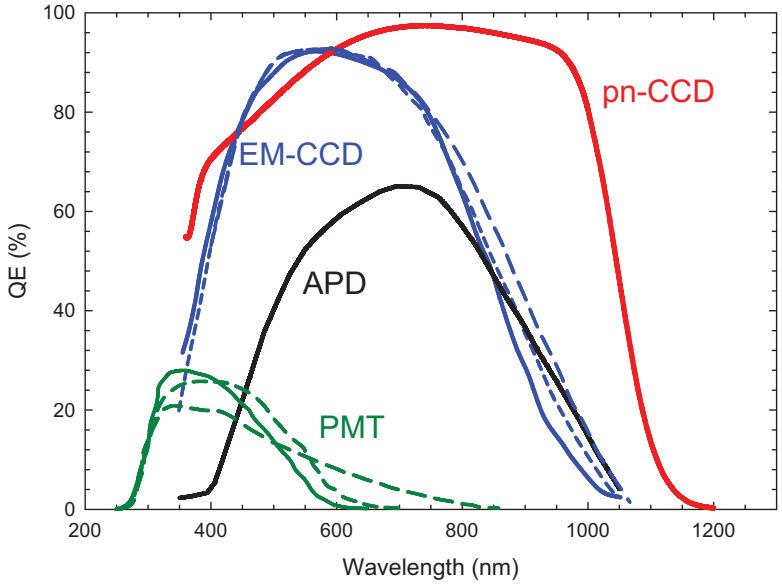

FIGURE 5. Generic quantum efficiency versus wavelength for different Si based detectors and PMTs. Shown are typical curves for single cell APDs, EM-CCDs, and pn-CCDs as well as different photocathodes in PMTs.

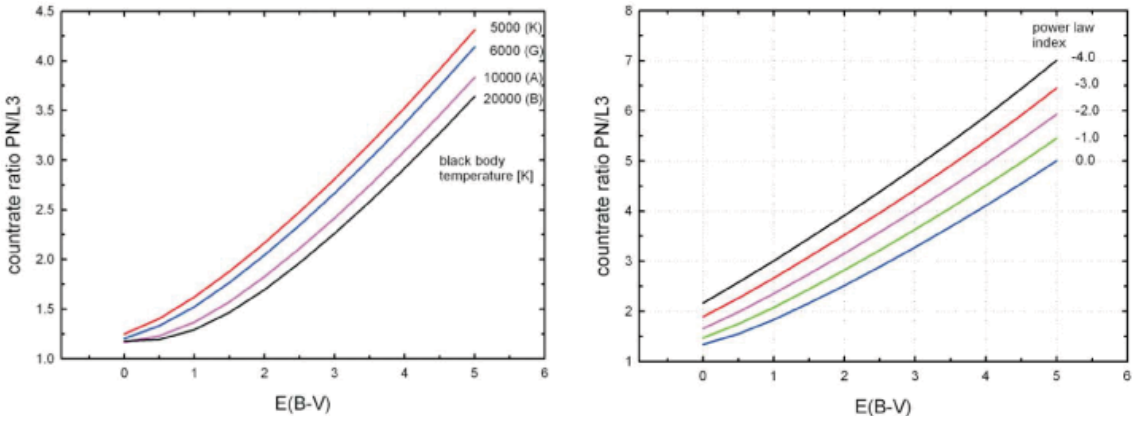

FIGURE 6. Gain in count rates for pnCCDs as compared to commercial back illuminated EM-CCDs. The left panel shows the count rate ratio for black body thermal spectra (typical stellar classification in parentheses) and on the right the results for power law spectra are given.

4. ENTRANCE WINDOW AND QUANTUM EFFICIENCY

Within our established double sided silicon technology, we are able to smoothly integrate a fully compatible back surface processing into the overall fabrication flow. Since our devices are back illuminated, this enables a full control over the radiation entrance window for further optimization at different wavelengths. Moreover, since the entrance window is unstructured it is sensitive over its full area resulting in a fill factor of 100 %.

As anti-reflective coating a homogeneous stack of layers, whose thicknesses can be

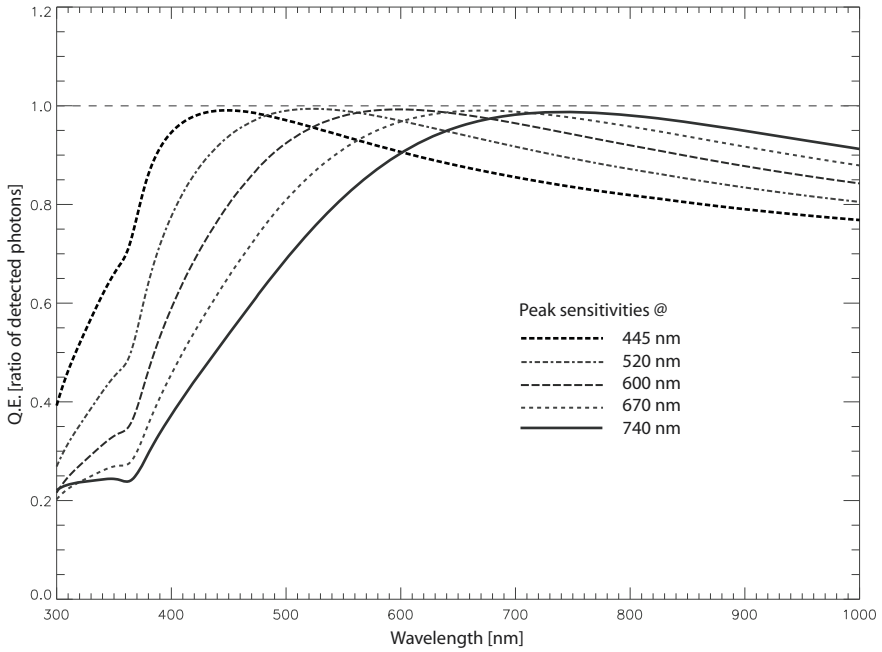

FIGURE 7. Simulated entrance window efficiencies obtained with different layer thicknesses.

controlled with high precision at process time, allows for different peak sensitivities from blue to red and NIR regimes. Figure 7 shows the result from a simulation for five different layer thicknesses. Peak sensitivities of almost 100 % are achieved in the 400-800 nm range, and are still above 90 % in the 800-1,000 nm region. More information on the simulations and also comparisons with measurements can be found e.g. in [3].

5. AVALANCHE READOUT

A single photon spectrum obtained with silicon photo-multiplier (SiPM) test structures is shown in Fig. 8. The signals are summed from 20 $\times$ 25 sub-pixels each having an avalanche region of 10 µm in diameter, which also represents the sensitive area. The peaks are very well separated and demonstrate the excellent uniformity of the avalanche signals and the technology. As photon source femto-second pulses from a laser were used. Details on this devices can be found in [4].

6. CONCLUSIONS

By making use of the full silicon wafer thickness to enhance the near infrared response, the improvement of the fabrication technology in terms of very low thermally generated leakage currents is essential to keep the number of dark counts low. We have shown that the number of electrons which are collected in a pixel of 50 µm $\times$ 50 µm on a 450 µm thick, fully depleted silicon can be kept at 10^{-2} electrons per pixel and second at an operating temperature of only -70°C. By adding adequate dielectrics as anti-reflective

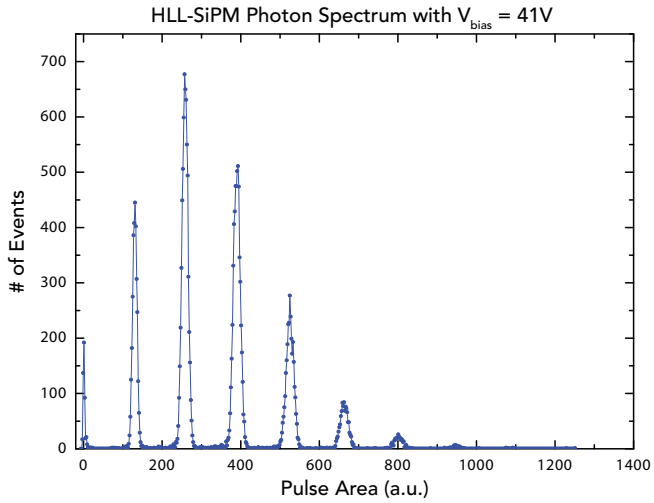

FIGURE 8. Photon spectrum recorded by SiPM test structures. The well separated peaks indicate events containing between one and seven photo-electrons. Since they are collected from 500 individual cells, the excellent uniformity of the technology is demonstrated.

coating a broad band response from 400 nm up to 1,100 nm was achieved. It was shown that the avalanche process is under control: the single photon measurements with the test structures were reproducible and stable with time. We have performed measurements with a high speed JFET amplifier based pnCCD camera with up to 2,400 frames per second on a telescope impressively proving the system concept and its performance. The full implementation of the avalanche structure and the on-chip amplifier is in production to fully exploit all properties in a single science grade device. In our midterm plans we have foreseen a fully optimized operational system to be used in dedicated optical and NIR observations.

ACKNOWLEDGMENTS

The authors like to thank Prof. Papamastorakis from University of Crete and the staff of the SKINAKAS observatory for their excellent support. We also thank the SiPM group and the electronics department of the Max-Planck-Institut für Physik for many fruitful discussions and their intense help in the testing.

REFERENCES

1. P. Holl, et al., “A New High-Speed, Single Photon Imaging CCD for the Optical,” *Conference record of IEEE Nuclear Science Symposium*, 2006.
2. S.Wölfel, et al., “A novel way of single photon detection: Beating 1/f noise limit with ultra high resolution DEPFET-RNDR devices,” *IEEE TNS, Vol. 54, No. 4, pp 1311 - 1318*, August 2007.
3. R.Hartmann, et al., “The Quantum Efficiency of pn-Detectors in the Spectral Range between 1 nm and 1000 nm,” *Nucl. Instr. & Meth. A, Vol. 439, pp 216 - 220*, 2000.
4. C.Merck, et al., “Back Illuminated Drift Silicon Photomultiplier as Novel Detector for Single Photon Counting,” *Conference record of IEEE Nuclear Science Symposium*, 2006.